

Effect of bridge lateral deformation on track geometry of high-speed railway

Hongye Gou^{*1,2}, Longcheng Yang^{1a}, Dan Leng^{1b}, Yi Bao^{3c} and Qianhui Pu^{1d}

¹ Department of Bridge Engineering, School of Civil Engineering, Southwest Jiaotong University, Chengdu 610031, China

² Key Laboratory of High-Speed Railway Engineering, Ministry of Education, Southwest Jiaotong University, Chengdu 610031, China

³ Department of Civil and Environmental Engineering, University of Michigan, Ann Arbor, MI 48109, USA

(Received April 18, 2018, Revised August 26, 2018, Accepted August 31, 2018)

Abstract. This paper presents an analytical model to analyze the mapping relationship between bridge lateral deformation and track geometry of high-speed railway. Based on the rail deformation mechanisms, the deformation of track slab and rail at the locations of fasteners are analyzed. Formulae of rail lateral deformation are derived and validated against a finite element model. Based on the analytical model, a rail deformation extension coefficient is presented, and effects of different lateral deformations on track geometry are evaluated. Parametric studies are conducted to evaluate the effects of the deformation amplitude, fastener stiffness and mortar layer stiffness on the rail deformation. The rail deformation increases with the deformation of the girder, and is dependent on the spacing of the fasteners, the elastic modulus of the rail's material, and the moment of inertia of the rail's section.

Keywords: analytical model; bridge lateral deformation; high-speed railway; mapping relationship; track geometry

1. Introduction

High-speed railway (HSR) has been constructed in many countries to improve the quality of life and facilitate development of economy (Hu *et al.* 2014, Rocha *et al.* 2014, Yan *et al.* 2015). By 2030, a HSR network that consists of eight vertical and eight horizontal main lines with a total mileage of more than 38,000 km will cover the main residential areas in China (He *et al.* 2017). With the expansion of the coverage area of HSR network, the operation environment of HSR is becoming more and more complex. The mileage of HSR is increasing in some areas with undesired or complicated geological conditions, seismically active zones and extreme climate regions (Chen *et al.* 2015). These environmental conditions tend to produce additional deformations of HSR bridges, such as pier settlement, creep camber, pier inclination, girder's rotation and lateral displacement, due to the external cyclic loading, degradation and creep of materials (Shao *et al.* 2016, Yang *et al.* 2014a, b, Deng *et al.* 2016, Wang *et al.* 2014, Strauss *et al.* 2017). Existing studies have shown that irreversible bridge deformations continue developing over time (Doménecha *et al.* 2014), and the effects of bridge deformation on railway track's geometry cannot be ignored, because the track's geometry directly affects the running

safety and riding comfort of trains (Ju *et al.* 2014, Yang *et al.* 2014b, Tutumluer *et al.* 2013, Kimani and Kaewunruen 2017). So, there is a need to understand the mapping relationship between the bridge deformation and the change of track geometry.

In recent decades, track-bridge interactions have been studied through a number of in-situ tests and laboratory experiments (Zhang *et al.* 2015, Yang and Jang 2016, Ruge *et al.* 2009, Toydemir *et al.* 2017, Olmos and Astiz 2013, Gou *et al.* 2018a-f). Chen *et al.* (2015) determined the safety threshold of bridge pier settlement for HSR according to the train-track-bridge dynamic interaction. Cai *et al.* (2017) established a finite element model to investigate the coupling behaviors of plate-type ballastless track-subgrade space. Guo (2016) presented a subgrade frost heave deformation transfer model, and studied the influence of different degrees of frost heaving deformation on the geometric deformation and interlayer contact of the rail. The measurement results of track irregularity showed that the track geometry is associated with the bridge deformation (Lian *et al.* 2007, Lee *et al.* 2012, Ma *et al.* 2014). Chen *et al.* (2014a, b) deduced the mapping relationship between the pier settlement and the rail deformation of HSR in the case of unit slab track system and longitudinal connected ballastless track system, and calculated the rail deformation curves using an analytic model. Statistical analyses have been conducted using test data and finite element models to study the relationship between the bridge pier or subgrade settlement and the track geometry (Chen *et al.* 2016, Jiang *et al.* 2012, Zou *et al.* 2014, Ju 2013, Gou *et al.* 2018g). However, the mapping relationship between bridge lateral deformation and track geometry has not been investigated yet.

The study aims to develop a practical analytical model for the mapping relationship between bridge lateral

*Corresponding author, Ph.D., Associate Professor,
E-mail: gouhongye@swjtu.cn

^a Master Student, E-mail: 1106461245@qq.com

^b Master Student, E-mail: 842006596@qq.com

^c Postdoctoral Research Fellow,
E-mail: yibao@umich.edu

^d Professor, E-mail: qhpu@vip.163.com

deformation and track geometry of HSR, and quantitatively study the influence of key parameters on the geometric shape change of the rail. The investigated parameters include the spacing of the fasteners, the elastic modulus of the rail's material, and the moment of inertia of the rail's section.

2. Development of analytical model

2.1 Mechanism analysis

In this study, the China Railway Track System (CRTS) I slab ballastless track structure is studied, as illustrated in Fig. 1. When lateral deformation of a bridge girder occurs, the base slab on the girder will deform with the girder, resulting in a relative deformation between the base slab and the upper slab. Such relative deformation will induce tension or compression in the CA mortar layer between the base and the slab. Meanwhile, due to the lateral constraint of the convex frame at the two ends of the track slab, compressive force is induced between the track slab and convex frame. Then the track slab produces a lateral deformation under the tension or compression of the mortar layer and the reaction force of the convex frame. The deformation will cause a relative deformation between the track slab and the rail, leading to the lateral force of the fastener. Finally, equilibrium will be achieved under the interaction effect of the track geometry and the deformation coordination effect (Poveda *et al.* 2015, Chen *et al.* 2014a).

The following five assumptions are introduced for the model development (Chen *et al.* 2014b).

- (1) The influence of the track deformation on bridge deformation is neglected.
- (2) The deformation of the base slab is the same as the deformation of the bridge girder.
- (3) The mortar layer, fastener and convex block filler can be modeled using linear springs.
- (4) Since the bending rigidity of the track slab in the lateral direction is much larger than that in the vertical direction, the lateral bending deformation of the track slab is neglected. Due to the small thickness of the track slab, the shear deformation is neglected.

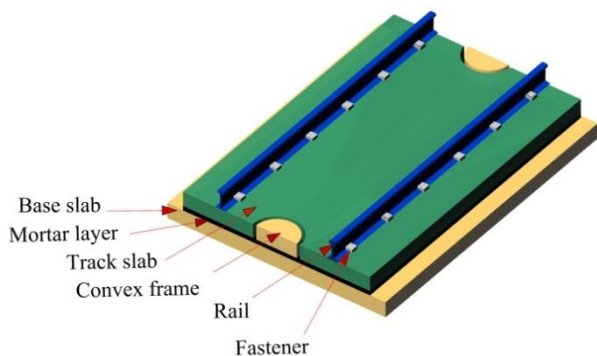


Fig. 1 China Railway Track System (CRTS) I slab ballastless track structure

- (5) The vertical, lateral and torsional deformation states of each interlayer structure are independent on each other.

2.2 Modelling of the track slab

Figs. 2(a) to (c) illustrate the forces applied on a track slab that is the m -th slab. When the girder has a lateral deformation (in the z_{ms} direction), the track slab is in equilibrium under the spring force ($R(x)$) of the mortar layer, the force (F_{mi}) of the convex frame, and the force (P_{mi}) from the fasteners. (Chen *et al.* 2014a). The number of the fasteners on the m -th track slab is $2n$, as shown in Fig. 2.

When the lateral deformation of bridge girder occurs, the forces (in Fig. 2) applied on the track slab are antisymmetry regarding to the center line of track slab (Yan 2015). Therefore, only a semi-structure of the track slab is studied in the force analysis.

Since the length and width of the track slab are much larger than the vertical height, the lateral bending stiffness of the track slab is much greater than the vertical bending stiffness. Therefore, only the lateral rigid body displacement of the track slab is considered in the calculation, and thus the deformation of track slab is a straight line. The lateral deformation function of the m -th track slab can be expressed as

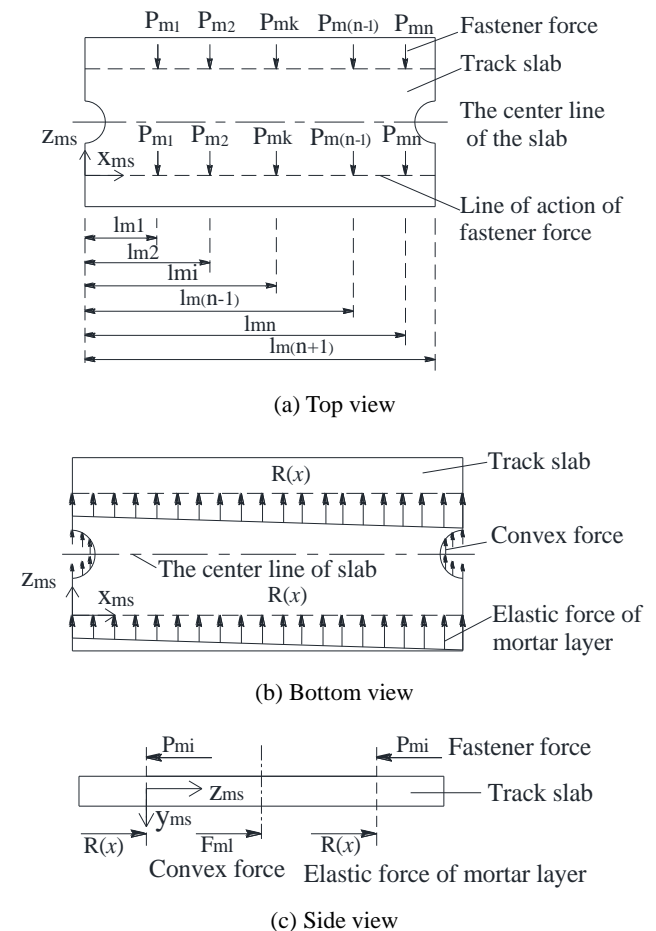


Fig. 2 Force analysis for the m -th track slab

$$z_{ms} = a_m x + b_m \quad (1)$$

where the values of a_m and b_m vary from track slab to track slab.

From Eq. (1), the deformation at the i -th fastener position of the track slab can be expressed as

$$z_{msi} = a_m l_{mi} + b_m \quad (2)$$

Particularly, the deformation of the left end of the track slab is $z_{ms0} = b_m$, and the right one is $z_{ms(n+1)} = a_m l_{m(n+1)} + b_m$.

The equation of equilibrium of the track slab in the lateral direction is

$$F_{ml} + F_{mr} + \sum_{k=1}^n P_{mk} + \int_0^{l_{m(n+1)}} R(x) dx = 0 \quad (3)$$

$$\int_0^{l_{m(n+1)}} R(x) x dx + \sum_{k=1}^n P_{mk} l_{mk} + F_{mr} l_{m(n+1)} = 0 \quad (4)$$

where $R(x) = k_{cz} [z_{ms}(x) - z_{mb}(x)]$.

By solving Eqs. (2) to (4), the deformation of the track slab at the i -th fastener of the m -th track slab can be obtained

$$\begin{aligned} z_{msi} = & \frac{c_{m3} - c_{m4} l_{mi}}{c_{m1} c_{m4} - c_{m2} c_{m3}} \sum_{k=1}^n P_{mk} + k_{cz} \frac{c_{m4} l_{mi} - c_{m3}}{c_{m1} c_{m4} - c_{m2} c_{m3}} \int_0^{l_{m(n+1)}} z_{mb} dx \\ & + \frac{c_{m2} l_{mi} - c_{m1}}{c_{m1} c_{m4} - c_{m2} c_{m3}} \sum_{k=1}^n P_{mk} l_{mk} + k_{cz} \frac{c_{m1} - c_{m2} l_{mi}}{c_{m1} c_{m4} - c_{m2} c_{m3}} \int_0^{l_{m(n+1)}} z_{mb} x dx \\ & + \frac{[c_{m4} k_t (z_{mb0} + z_{mb(n+1)}) - c_{m2} k_t z_{mb(n+1)} l_{m(n+1)}] l_{mi}}{c_{m1} c_{m4} - c_{m2} c_{m3}} \\ & + \frac{c_{m1} k_t z_{mb(n+1)} l_{m(n+1)} - c_{m3} k_t (z_{mb0} + z_{mb(n+1)})}{c_{m1} c_{m4} - c_{m2} c_{m3}} \end{aligned} \quad (5)$$

$$\begin{aligned} \text{where } c_{m1} = & k_t l_{m(n+1)} + \frac{k_{cz} l_{m(n+1)}^2}{2}, \quad c_{m2} = 2k_t \\ & + k_{cz} l_{m(n+1)}, \quad c_{m3} = k_t l_{m(n+1)}^2 + \frac{k_{cz} l_{m(n+1)}^3}{3}, \quad c_{m4} = \\ & k_t l_{m(n+1)} + \frac{k_{cz} l_{m(n+1)}^2}{2}. \end{aligned}$$

Based on Eq. (5), the deformation at the position of all the fasteners of the m -th track slab is expressed as a matrix

$$[\mathbf{Z}_{ms}] = [\mathbf{A}_m][\mathbf{P}_m] + [\mathbf{T}_m] \quad (6)$$

where, $[\mathbf{z}_{ms}]$, $[\mathbf{T}_m]$ and $[\mathbf{P}_m]$ are $n \times 1$ matrices, $[\mathbf{A}_m]$ is an $n \times n$ matrix. The matrix elements are in Eqs. (7) to (10)

$$\mathbf{Z}_{ms}(k, 1) = z_{msk} \quad (7)$$

$$\begin{aligned} \mathbf{T}_m(k, 1) = & \frac{[c_{m4} k_t (z_{mb0} + z_{mb(n+1)}) - c_{m2} k_t z_{mb(n+1)} l_{m(n+1)}] l_{mi}}{c_{m1} c_{m4} - c_{m2} c_{m3}} \\ & + \frac{c_{m1} k_t z_{mb(n+1)} l_{m(n+1)} - c_{m3} k_t (z_{mb0} + z_{mb(n+1)})}{c_{m1} c_{m4} - c_{m2} c_{m3}} \\ & + k_{cz} \frac{c_{m4} l_{mi} - c_{m3}}{c_{m1} c_{m4} - c_{m2} c_{m3}} \int_0^{l_{m(n+1)}} z_{mb} dx \\ & + k_{cz} \frac{c_{m1} - c_{m2} l_{mi}}{c_{m1} c_{m4} - c_{m2} c_{m3}} \int_0^{l_{m(n+1)}} z_{mb} x dx \end{aligned} \quad (8)$$

$$\mathbf{A}_m(k, j) = \frac{c_{m3} - c_{m4} l_{mk} + (c_{m2} l_{mk} - c_{m1}) l_{mj}}{c_{m1} c_{m4} - c_{m2} c_{m3}} \quad (9)$$

$$\mathbf{P}_m(k, 1) = P_{mk} \quad (10)$$

where $k = 1, 2, \dots, n; j = 1, 2, \dots, n$.

The bridge has M spans, each of the M spans has N track slabs. Therefore, the total number of the track slabs is $M \times N$. The total number of fasteners is denoted as sum . The deformation of the track slab at all of the fasteners on the track slabs are expressed in a matrix form

$$[\mathbf{Z}_s] = [\mathbf{A}][\mathbf{P}] + [\mathbf{T}] \quad (11)$$

where $[\mathbf{Z}_s]$, $[\mathbf{A}]$ and $[\mathbf{P}]$ are $sum \times 1$ -order matrices; $[\mathbf{T}]$ is a $sum \times sum$ -order matrix.

2.3 Modelling of the rail

An infinite beam model with an elastic support is used to investigate the deformation of the rail, as shown in Fig. 3. An arbitrary rail segment between two fasteners is selected to analyze the deformation of the rail. Since there is no external load between the two ends of the rail segment, the shear force in the rail segment is constant between the two fasteners.

Fig. 4 illustrates the shear force and moment at the two ends of the rail segment. A local coordinate system (x, z) is used for mechanical analysis, where $x \in [0, l_{t+1} - l_t]$.

Based on the approximate differential equation of the deflection curve of the girder, the relationship between shear force and deformation can be expressed as

$$-EI_{rz} \frac{d^3 z}{dx^3} = Q_t \quad (12)$$

According to the boundary conditions at $x = 0$ (Fig. 4), the deformation of the rail is z_t , the angle between the x axis and the tangent line of the rail deformation curve is ϕ_t , the

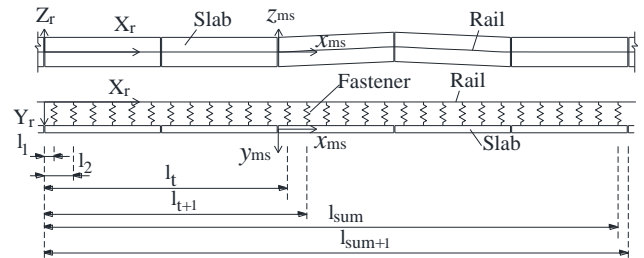


Fig. 3 Schematic diagram of rail lateral deformation

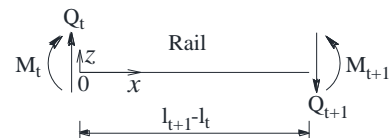


Fig. 4 Force diagram of the rail

bending moment is M_t , the shear is Q_t , the expression of rail deformation can be written as

$$z(x) = z_t + \varphi_t x - \frac{M_t}{2EI_{rz}} x^2 - \frac{Q_t}{6EI_{rz}} x^3 \quad (13)$$

Due to the length of the rail analysis zone is greater than that of bridge structure deformation zone (Fig. 3), the boundary conditions of the rail at $X_r = 0$ and $X_r = l_{sum+1}$ have negligible influence on the overall behavior of the rail caused by the deformation of the bridge. Therefore, the simply supported rail is employed in this study. When X_r is equal to zero, the rail deformation (Z_{r0}) and the bending moment (M_{r0}) are equal to zero; when X_r is equal to l_{sum+1} , the rail deformation ($Z_{r(sum+1)}$) and the bending moment ($M_{r(sum+1)}$) are equal to zero.

According to Eq. (13), with the linear superposition principle and the boundary conditions of the rail, the deformation of the rail at the position of the t -th fastener is given by

$$Z_{rt} = l_t \varphi_{r0} - \frac{l_t^3}{6EI_{rz}} Q_{r0} - \sum_{k=1}^t \frac{(l_t - l_k)^3}{6EI_{rz}} (-P_k) \quad (14)$$

The expression of moment at the position of the t -th fastener is

$$M_{rt} = l_t Q_{r0} - \sum_{k=1}^t (l_t - l_k) P_k \quad (15)$$

Based on the boundary conditions at $X_r = l_{sum+1}$ and the Eqs. (14) and (15), the rotating angle (φ_{r0}) and the shear force (Q_{r0}) can be obtained

$$\varphi_{r0} = \sum_{k=1}^{sum} \frac{l_{sum+1}^2 (l_{sum+1} - l_k) - (l_{sum+1} - l_k)^3}{6EI_{rz} l_{sum+1}} P_k \quad (16)$$

$$Q_{r0} = \sum_{k=1}^{sum} \frac{(l_{sum+1} - l_k)}{l_{sum+1}} P_k \quad (17)$$

Substituting Eqs. (16) and (17) in Eq. (14), the deformation at the position of the t -th fastener is given by

$$Z_{rt} = l_t \sum_{k=1}^{sum} \frac{l_{sum+1}^2 (l_{sum+1} - l_k) - (l_{sum+1} - l_k)^3}{6EI_{rz} l_{sum+1}} P_k - l_t^3 \sum_{k=1}^{sum} \frac{(l_{sum+1} - l_k)}{6EI_{rz} l_{sum+1}} P_k + \sum_{k=1}^t \frac{(l_t - l_k)^3}{6EI_{rz}} P_k \quad (18)$$

The deformation value of the rail at all the fastener positions can be expressed in a matrix form

$$[\mathbf{Z}_r] = [\mathbf{H}][\mathbf{P}] \quad (19)$$

where $[\mathbf{Z}_r]$ and $[\mathbf{H}]$ are $sum \times sum$ -order matrices, and the matrix element expression is

$$\mathbf{Z}_r(t, 1) = Z_{rt} \quad (20)$$

$$\mathbf{H}(t, k) = \frac{l_t l_{sum+1}^2 (l_{sum+1} - l_k) - l_t (l_{sum+1} - l_k)^3}{6EI_{rz} l_{sum+1}} - \frac{l_t^3 (l_{sum+1} - l_k) - (l_t - l_k)^3}{6EI_{rz} l_{sum+1}} \quad (21)$$

$(t \geq k, t = 1, 2, \dots, sum; k = 1, 2, \dots, sum)$

2.4 Analytical expression of mapping relationship

As an important interlayer connection structure for HSR ballastless track, fastener has an important limitation and effect on rail deformation. According to the relationship between the fastener force and the deformation of track slab and rail, the fastener force matrix can be summarized by the following

$$[\mathbf{P}] = k_{fc} ([\mathbf{Z}_s] - [\mathbf{Z}_r]) \quad (22)$$

From Eqs. (11), (19) and (22), the following equation can be obtained

$$[\mathbf{P}] = ([\mathbf{I}] - k_{fc} [\mathbf{A}] + k_{fc} [\mathbf{H}])^{-1} k_{fc} [\mathbf{T}] \quad (23)$$

where $[\mathbf{I}]$ is a $sum \times sum$ -order identity matrix.

According to Eqs. (19) and (23), the analytical matrix of the mapping relationship between the lateral deformation of the bridge structure and the track geometry at all fastener positions is

$$[\mathbf{Z}_r] = [\mathbf{H}] ([\mathbf{I}] - k_{fc} [\mathbf{A}] + k_{fc} [\mathbf{H}])^{-1} k_{fc} [\mathbf{T}] \quad (24)$$

In this equation, the elements in the influence matrix $[\mathbf{T}]$ are only related to the function of the bridge structure deformation. Therefore, the influence of girder's lateral end rotation and fault on the track geometry are only reflected on the matrix $[\mathbf{T}]$.

Furthermore, the lateral deformation of the rail at all positions can be solved by Eq. (25)

$$Z_{rt}(X_r) = \varphi_{r0} X_r - \frac{Q_{r0}}{6EI_{rz}} X_r^3 + \sum_{k=1}^t \frac{(X_r - l_k)^3}{6EI_{rz}} P_k \quad (25)$$

where $l_t \leq X_r < l_{t+1}$, $t = 1, 2, \dots, sum$.

2.5 Program implementation

According to the mapping relationship between the lateral deformation of the bridge and the track geometry, MATLAB is used to program the mapping relationship. The 5-span 32-m high-speed railway simply supported bridge and the upper CRTS I slab ballastless track structure are taken as the prototype to solve the rail deformation under the lateral girder fault and lateral girder end rotation deformation.

Table 1 Main calculation parameters of the CRTS I ballastless track slab and the bridge

Structure	Materials	Elastic modulus, E (MPa)	Moment of inertia of cross-section, I_{yy} (mm ⁴)	Lateral spring stiffness	
				Finite element model	Mapping model
Rail	U71MnG	2.10×10^5	5.240×10^6	—	—
Track slab	C60 concrete	3.65×10^4	2.189×10^{11}	—	—
Base slab	C40 concrete	3.40×10^4	3.614×10^{11}	—	—
Girder	C50 concrete	3.55×10^4	8.754×10^{13}	—	—
Filling resin	Polyurethane resin	—	—	2.6×10^6 N/m	1.3×10^6 N/m
Mortar layer	CA mortar	—	—	1.2×10^8 N/m ²	3.9×10^8 N/m ²
Fastener	WJ-7B	—	—	5.0×10^7 N/m	5.0×10^7 N/m

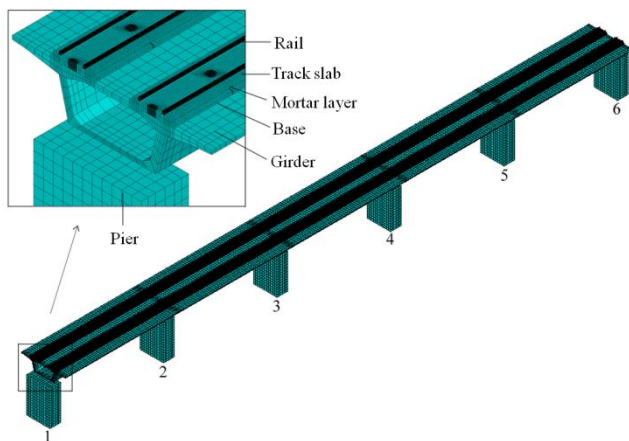


Fig. 5 Finite element model of the CRTS I slab ballastless track and the bridge

3. Model validation and discussion

Taking two typical deformation modes of lateral girder fault and lateral girder end rotation as an example, the rail deformation, the fastener force and the deformation length of rail at different bridge deformation modes are obtained. Some studies have shown that it is accurate and effective to use the FE model to solve the mapping relationship between the deformation of the girder and the deformation of the rail. (Chen *et al.* 2014b, Lei 2001, Olmos and Astiz 2013). Therefore, the effectiveness of the mapping model is verified by comparing the results of the FE model and the mapping model.

3.1 Finite element model

In this paper, ANSYS was used to model the CRTS I ballastless track slab and the bridge, as shown in Fig. 5. The rail was simulated by the space girder element BEAM188. The track slab, base, girder and the convex retaining platform were simulated by the solid element SOLID45. The fastener and the resin filled layer were simulated by 3-D spring element COMBIN14. The mortar layer was simulated by the element COMBIN14 which arranged along the center line of the rail with 1/2 spacing of fasteners. The bridge bearing was constrained by the master-slave degree of freedom. The fixed end constraint was applied at the bottom of the pier and at the end of the

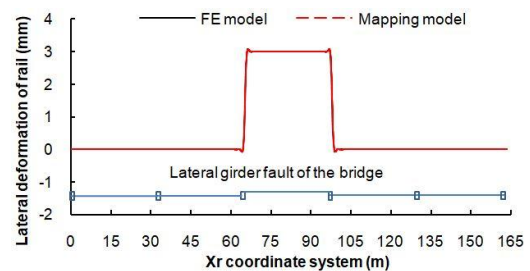


Fig. 6 Rail deformation under a lateral girder fault of 3 mm

rail. The girder lateral end rotation and fault were constrained by the degree of freedom. The deadweight of the structure was ignored.

The main calculation parameters of the girder and the CRTS I ballastless track slab were shown in Table 1. In the FE model, the stiffness of the mortar layer was the product of the spring stiffness and 1/2 spacing of fasteners.

3.2 Comparison between the proposed Model and the FE model

3.2.1 Lateral girder fault

This section analyzed the deformation of the lateral girder fault of the bridge. It is assumed that there is a lateral girder fault of 3 mm in the third span (Fig. 5). The rail deformation is analyzed by the FE model and the mapping model, as shown in Fig. 6.

It can be seen in Fig. 6 that the deformation curves obtained by the FE model and the mapping model are basically coincident. The track geometry is symmetrical with respect to the third span. The rail deformation is in agreement with the result of girder in the area of the lateral girder fault and decreases rapidly when it is far away from the lateral fault area. The curves are smooth without obvious sharp angle when passing the girder fault area.

The forces of all fasteners are shown in Fig. 7. It can be seen in Fig. 7 that the fastener forces obtained by the FE model and the mapping model coincides well. The absolute deviation is not more than 0.15 kN. The fasteners forces are symmetrical with respect to the center of the lateral fault area. The forces are large when passing the fault area and they are antisymmetric with respect to the center line of the girder seams at the pier No. 3 and No. 4. The deformation trend is consistent with those of the girder and rail. There-

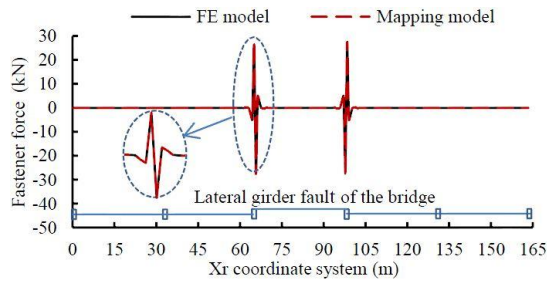


Fig. 7 Fastener force under a lateral girder fault of 3 mm

fore, both methods can be used to solve the mapping relationship between the lateral girder fault and the rail deformation for the slab ballastless track. Compared with the FE model, the mapping model can better describe the relationship between the parameters and rail deformation, and it can greatly shorten the time of modeling.

3.2.2 Lateral girder end rotation

It is assumed that there is a symmetrically lateral rotation of 1‰ rad in the third and the fourth span (Fig. 5). The rail deformation is analyzed by the FE model and the mapping model, as shown in Fig. 8.

Fig. 8 shows the curves of the rail deformations that are obtained by the FE model and the mapping model. They are basically coincident. The track geometry is symmetrical with respect to the third pier. The rail deformation is consistent with the girder deformation in the area of the girder's lateral rotation and decreases rapidly when it is far away from the lateral rotation. The rail deformation curves

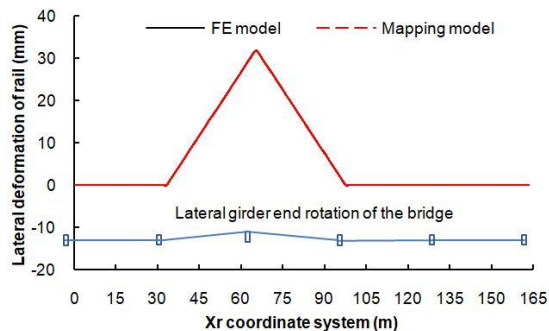


Fig. 8 Rail deformation under a lateral girder end rotation of 1‰ rad

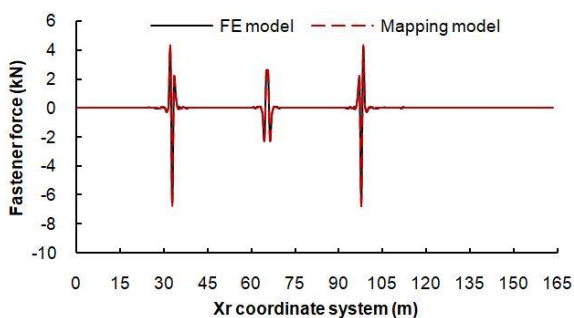


Fig. 9 Fastener force under a lateral girder end rotation of 1‰ rad

Table 2 Comparison of elongation coefficients of rail deformation at different bridge lateral deformation

Rail deformation	3 mm lateral girder fault	0.1‰ rad lateral girder end rotation
Elongation coefficients	1.103	1.006

are smooth without obvious sharp angle when passing the lateral girder end rotation area. It shows that both methods can be used to analyze the mapping relationship between the lateral girder end rotation and the rail deformation for the slab ballastless track.

Due to the rail directly bears the fasteners force, its geometry is closely related to the fasteners force state. Forces of the whole fasteners under the lateral girder end rotation of 1‰ rad are shown in Fig. 9. It can be seen in Fig. 9 that the fasteners forces obtained by the FE model has a close agreement with the value attained by the mapping model. The absolute deviation is less than 0.05 kN. The fastener forces are symmetrical with respect to the pier No. 3. The forces are large at the end of the second and the third girders. Away from the end of the girder, the fastener forces approach to zero. The deformation trend is consistent with those of girder and rail.

In summary, under the condition of lateral girder fault and lateral girder end rotation, the rail deformation trend and the fasteners forces obtained by the FE model and the mapping model are basically consistent. Therefore the mapping model is effective and reliable.

3.3 Mapping effects of different lateral deformation on track geometry

To study the mapping effect of different bridge lateral deformation on track surface, the elongation coefficients of rail deformation with 3 mm lateral girder fault and 0.1‰ rad lateral girder end rotation (the maximum girder deformation is about 3 mm) are compared and analyzed as shown in Table 2. It shows that the elongation coefficients are different when the maximum girder deformations are close. The elongation coefficient of lateral girder fault is larger than that of lateral girder end rotation, which shows that the mapping effect of lateral girder fault is greater than that of lateral girder end rotation. This is mainly influenced by the smoothness of the rail deformation transition curve when passing the deformation area of the bridge.

4. Effects of model parameters on track geometry

4.1 Bridge lateral deformation amplitude

4.1.1 Lateral girder fault

In order to study the influence of the lateral girder fault amplitude on the rail surface deformation, the fault amplitude of the third span (see Fig. 5) was analyzed under five different conditions of 0.5 mm, 1 mm, 2 mm, 3 mm, and 4 mm. The deformation trend of the rail, the maximum value of the deformation, and the rail deformation area

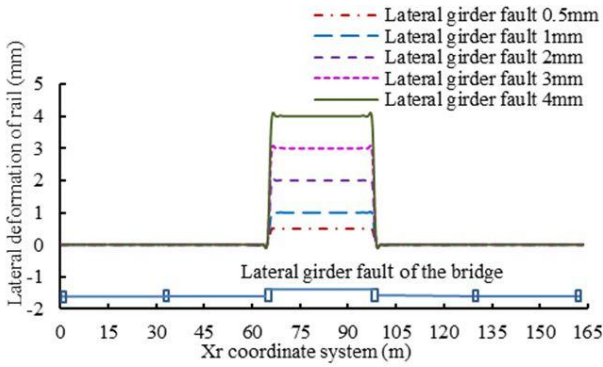


Fig. 10 Rail deformation diagram of different lateral girder fault

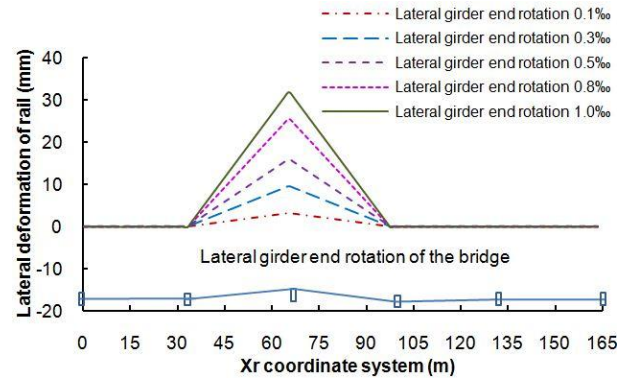


Fig. 12 Rail deformation diagram of different lateral girder end rotation

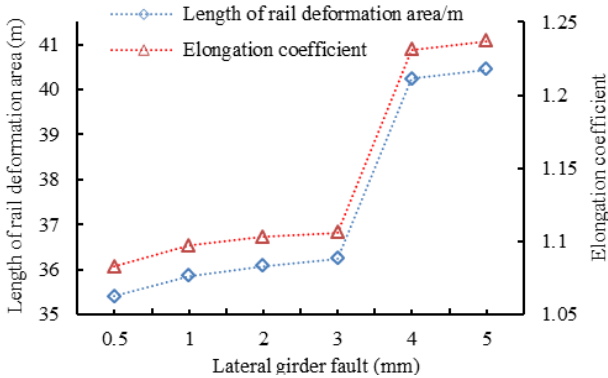


Fig. 11 Relationship between the rail deformation characteristic and the lateral girder fault

length were contrasted and analyzed.

Fig. 10 shows the overall deformation of the rail and the details of the rail deformation. It can be concluded that in the area of the lateral girder fault, the deformations of the rail and the girder are similar, with the increase of the amplitude, the rail deformation is larger. The deformation of rail decreases rapidly far away from the girder fault, and it is not affected by the amplitude of lateral fault. The rail is upturned and concave when passing the girder fault, but the transition curve is moderate. While with the increase of the amplitude, the upward and concave phenomena of the rail are more remarkable.

To study the regional effect of rail deformation caused by lateral girder fault, where the deformation exceeds 0.01mm is defined as the rail deformation area. In order to study the mapping effect of bridge deformation to the rail, the ratio of the length of the rail deformation area to the length of the girder deformation area is defined as the elongation coefficient of the rail deformation. The rail deformation area and rail deformation elongation coefficient are shown in Fig. 11. It can be concluded that the length of the rail deformation area increases with the increase of the lateral girder fault value. When the lateral girder fault value is less than 3 mm, the elongation coefficient is between 1.08~1.25, the variation of the amplitude has no obvious effect on the length of rail deformation area. The length of rail deformation area increases abruptly while the value of the lateral girder fault

is greater than 3 mm but less than 4 mm. When the amplitude is greater than 4 mm, the girder fault has little effect on the length of the rail deformation area.

4.1.2 Lateral girder end rotation

This section focuses on the effect of lateral girder end rotation on rail surface deformation. The amplitudes of the lateral girder end rotation were divided into five conditions (0.1‰ rad, 0.3‰ rad, 0.5‰ rad, 0.8‰ rad, and 1‰ rad) to analyze the rail deformation and the elongation coefficients of rail deformation as shown in Fig. 12. The deformation trend of the rail is similar under these five different conditions. In the area of the lateral rotation, the deformations of the rail and the girder are similar. With the increase of the amplitude, the rail deformation is larger. The deformation of the rail decreases rapidly far away from the lateral rotation, and it is not affected by the lateral rotation. When passing the lateral end rotation and the pier No. 3, the rail presents a lateral folded angle. With the increase of the amplitude, the folded angle is more obvious, and the deformation of the rail increases correspondingly.

The relationship between the length of rail deformation area and elongation coefficient of the rail deformation are demonstrated in Fig. 13. With the increase of lateral girder end rotation amplitude the length of rail deformation area and elongation coefficient increase gradually. When the amplitude is less than 0.3‰ rad, the length of rail deforma-

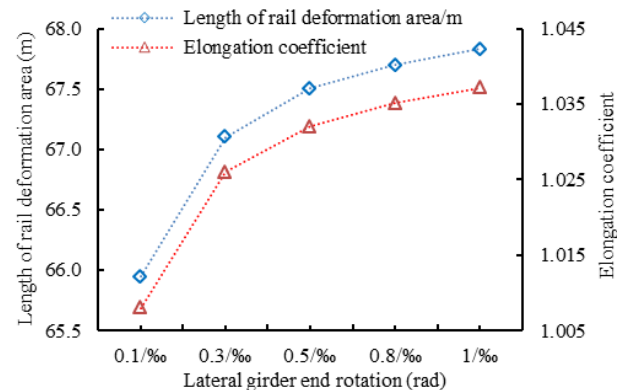


Fig. 13 Relationship between the rail deformation characteristic and the lateral girder end rotation

tion area and the elongation coefficient increase sharply. When the amplitude is more than 0.3‰ rad, the growth rate slow down gradually. In general, the rail deformation elongation coefficient is between 1.00~1.04. Under the two different deformation modes of bridge structure, the rail deformation is linear with the amplitude of bridge deformation. The deformation elongation coefficient of rail increases with the bridge deformation amplitude. Considering the force balance of the interlayer structure, the alternation of tension and pressure stress appears, thus leading to the deformation trend of the microwave wave shape of the rail. With the increase of amplitude, if a bigger difference between the adjacent fastener force values away from the deformation area of bridge, the rail deformation will not be neglected, which may lead to a sudden increase of elongation coefficient of rail deformation. However, the force of ballastless track structure caused by the deformation of bridge structure is mainly concentrated in the range of several fasteners spacing at the end of girder, and the force decreases rapidly with the increasing distance from the girder end. Therefore, the elongation coefficient increases slowly with the deformation amplitude of bridge structure.

4.2 Fastener stiffness

As an important intermediate connection between the rail and the substructure of the rail, fastener has a direct effect on the rail deformation. Therefore six fasteners with different lateral stiffness (10, 25, 35, 45, 55, and 75 kN/mm) were analyzed in this section. The lateral girder fault of 3 mm was considered the deformation conditions; the additional deformation of the rail was compared with different fastener stiffness. Fig. 14 shows the relationship between the rail deformation and the fastener stiffness.

It can be seen from Fig. 14, when the fastener stiffness is less than 35 kN/mm, with the increase of fastener stiffness, the length of the rail deformation area and the elongation coefficient decrease gradually. However when the lateral stiffness is greater than 45 kN/mm, the effect of the lateral stiffness on the elongation coefficient is not remarkable. This is mainly caused by the matching of fastener stiffness and mortar layer stiffness. When the fastener stiffness is small, the integrity of track slab, mortar

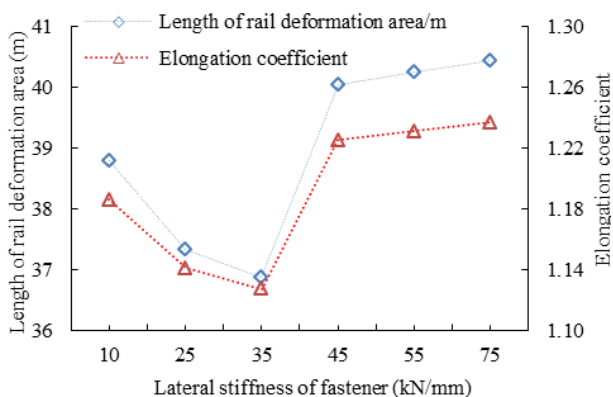


Fig. 14 The relationship between the rail deformation and the fastener stiffness

layer and girder body are relatively strong, that is, the deformation of track slab is mainly controlled by its substructure. Therefore, increasing the stiffness of fastener, the rail deformation area will gradually decrease. When the fastener stiffness is large, the connection of rail, track slab and fastener are enhanced, the deformation of track slab is mainly controlled by fastener force. Thus increasing the stiffness of fastener, the track slab deformation will cause greater fastener force. According to the lateral force balance of the track slab and the rigid deformation assumption, the force of fastener at the other end of the track slab is larger. Due to the deformation coordination effect between fastener and rail, the fastener force will affect those at the end of the next track slab through the rail deformation, and then the length of the rail deformation area is affected.

4.3 Mortar layer stiffness

The deformation of track slab can be restricted by mortar layer when the deformation of bridge structure is occurred. The deformation of the track slab will be reflected on rail by the fastener force, so the mechanical properties of mortar layer have an indirect influence on rail deformation. In this section, six types of mortar with different lateral stiffness (10, 50, 100, 150, 250, and 450 kN/mm) were utilized to analyze the rail deformation.

The characteristics of the rail deformation with different lateral stiffness of the mortar layer under the condition of lateral girder fault of 3 mm are shown in Fig. 15. It can be seen that with the increase of the lateral stiffness of the mortar layer, the length of the deformation area and the maximum value of rail deformation decrease gradually. When the lateral stiffness of the mortar layer is less than 100 kN/mm, increasing the stiffness, the elongation coefficient of the rail will decrease rapidly. When the lateral stiffness is greater than 100 kN/mm, the effect of the lateral stiffness on the elongation coefficient is not remarkable.

The results show that when the lateral deformation occurs in the bridge structure, increasing the stiffness of mortar layer, the interlayer structure of ballastless track will be enhanced. Therefore, the length of the rail deformation area decreases and the deformation curve of the rail become steeper, which influence the train operation.

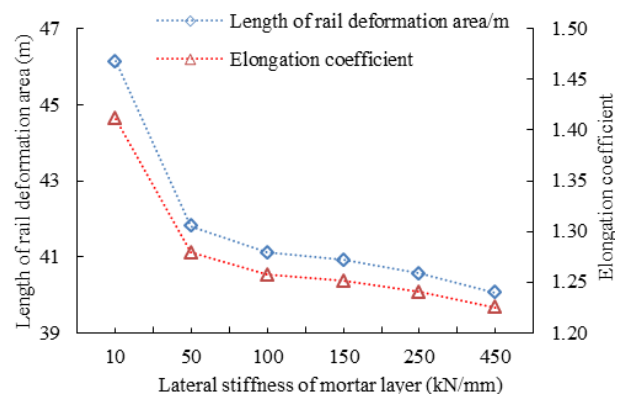


Fig. 15 The relationship between the rail deformation and the mortar layer stiffness

5. Conclusions

The following conclusions can be drawn:

- The rail deformation is obviously consistent with the girder deformation in the bridge deformation area. Away from the girder deformation area, the rail deformation decreases remarkably. When passing and out of the deformation area, the deformation curve of the rail is smooth without obvious sharp angle.
- The maximum value of the rail deformation is linearly related to the bridge deformation amplitude. Increasing the deformation amplitude of the bridge, the rail deformation will be enhanced.
- The fastener stiffness has an influence on the rail deformation. The smaller the fastener stiffness is, the flatter the rail deformation curve is, and the stronger the rail follows the deformation of the bridge structure.
- The stiffness of mortar layer also affects the rail deformation. The greater the stiffness of the mortar layer is, the stronger the interaction between the interlayer structures of the ballastless track is, the worse the performance of the rail following the deformation of the bridge structure, the steeper the rail deformation curve is, causing the train operation performance will be worse.

Acknowledgments

The research described in this paper was financially supported by the National Natural Science Foundation of China (Grant numbers 51878563), the Sichuan Science and Technology Program (Grant number 2018JY0294 and 2018JY0549), and the Science and Technology Research and Development Plan of China Railway Construction (Grant number 2014-C34).

References

- Cai, X.P., Liang, Y.K., Tan, S.Y. and Shen, Y.P. (2017), "Deformation and seam characteristics analysis of CRTS I slab ballastless track in subgrade frost heaving zone", *J. Beijing Jiaotong Univ.*, **41**(1), 7-13.
- Chen, X.P., Wang, F.F. and Zhao, C.Y. (2014a), "Fracture influence of longitudinal-continuous base layer on force characteristics of CRTS II slab ballastless track on bridge", *J. Traffic Transport. Eng.*, **14**(4), 25-35.
- Chen, Z.W., Sun, Y. and Zhai, W.M. (2014a-b), "Mapping relationship between pier settlement and rail deformation of high-speed railways-part (I): The unit slab track system", *Sci. China: Technol. Sci.*, **44**(7), 770-777. [In Chinese]
- Chen, Z.W., Sun, Y. and Zhai, W.M. (2014b-c), "Mapping relationship between pier settlement and rail deformation of high-speed railways-part (II): The longitudinal connected ballastless track system", *Sci. China: Technol. Sci.*, **44**(7), 778-785. [In Chinese]
- Chen, Z.W., Zhai, W.M., Cai, C.B. and Sun, Y. (2015), "Safety threshold of high-speed railway pier settlement based on train-track-bridge dynamic interaction", *Sci. China Tech. Sci.*, **58**, 202-210.
- Chen, Z.W., Zhai, W.M. and Yin, Q. (2016), "Analysis of structural stresses of tracks and vehicle dynamic responses in train-track-bridge system with pier settlement", *P. I. Mech. Eng. F-J. Rai.*, **232**(2), 421-434.
- Deng, J., Liu, A., Yu, Q. and Peng, G. (2016), "Seismic performances of steel reinforced concrete bridge piers", *Steel Compos. Struct., Int. J.*, **21**(3), 661-677.
- Doménecha, A., Muserosb, P. and Martínez-Rodrigoa, M.D. (2014), "Influence of the vehicle model on the prediction of the maximum bending response of simply-supported bridges under high-speed railway traffic", *Eng. Struct.*, **72**, 123-139.
- Gou, H.Y., Long, H., Bao, Y., Chen, G., Pu, Q. and Kang, R. (2018a), "Experimental and numerical studies on stress distributions in girder-arch-pier connections of long-span continuous rigid frame arch railway bridge", *J. Bridge Eng.*, **23**(7), 04018039.
- Gou, H.Y., Wang, W., Shi, X.Y., Pu, Q. and Kang, R. (2018b), "Behavior of steel-concrete composite cable anchorage system", *Steel Compos. Struct., Int. J.*, **26**(1), 115-123.
- Gou, H.Y., He, Y.N., Zhou, W., Bao, Y. and Chen, G. (2018c), "Experimental and numerical investigations of the dynamic responses of an asymmetrical arch railway bridge", *P. I. Mech. Eng. F-J. Rai.* DOI: 10.1177/0954409718766929.
- Gou, H.Y., Zhou, W., Bao, Y., Li, X.B. and Pu, Q. (2018d), "Experimental study on dynamic effects of a long-span railway continuous beam bridge", *Appl. Sci.*, **8**(5), 669. DOI: 10.3390/app8050669
- Gou, H.Y., Zhou, W., Chen, G., Bao, Y. and Pu, Q. (2018e), "In-situ test and dynamic analysis of a double-deck tied-arch bridge", *Steel Compos. Struct., Int. J.*, **27**(2), 161-175.
- Gou, H.Y., Shi, X., Zhou, W., Cui, K. and Pu, Q. (2018f), "Dynamic performance of continuous railway bridges: Numerical analyses and field tests", *P. I. Mech. Eng. F-J. Rai.*, **232**(3), 936-955.
- Gou, H.Y., Ran, Z.W., Yang, L.C., Bao, Y. and Pu, Q. (2018g), "Mapping Vertical Bridge Deformations to Track Geometry for High-speed Railway", *Steel Compos. Struct., Int. J.* [Under review]
- Guo, Y. (2016), "Study on the effect of subgrade frost heaving on the deformation properties of track structure and its vehicle dynamic behavior in high-speed railway", M.S. Dissertation; Southwest Jiaotong University, Chengdu, China.
- He, X., Wu, T., Zou, Y., Chen, Y.F. and Guo, H. (2017), "Recent developments of high-speed railway bridges in China", *Struct. Infrastruct. E.*, **13**(12), 1584-1595.
- Hu, N., Dai, G.L., Yan, B. and Liu, K. (2014), "Recent development of design and construction of medium and long span high-speed railway bridges in China", *Eng. Struct.*, **74**, 233-241.
- Jiang, L.F., Xiong, S.D., Xu, X.C. and Chen, S.X. (2012), "Study on the Evaluation Method of Subgrade Settlement Caused by Structure Layer of the High-Speed Railway", *Appl. Mech. Mater.*, **188**, 72-77.
- Ju, S.H. (2013), "3D analysis of high-speed trains moving on bridges with foundation settlements", *Arch. Appl. Mech.*, **83**, 281-291.
- Ju, S.H., Leong, C.C. and Ho, Y.S. (2014), "Safety of maglev trains moving on bridges subject to foundation settlements and earthquakes", *J. Bridge Eng.*, **19**(1), 91-100.
- Kimani, S.K. and Kaewunruen, S. (2017), "Free vibrations of precast modular steel-concrete composite railway track slabs", *Steel Compos. Struct., Int. J.*, **24**(1), 113-128.
- Lee, J.S., Choi, S., Kim, S.S., Kim, Y.G. and Kim, S.W. (2012), "Waveband analysis of track irregularities in high-speed railway from on-board acceleration measurement", *J. Solid Mech.*

Mater. Eng., **6**(6), 750-759.

- Lei, X. (2001), "Dynamic analysis of the track structure of a high-speed railway using finite elements", *P. I. Mech. Eng. F-J. Rai.*, **215**(4), 301-309.
- Lian, S.L., Liu, Y. and Yang, W.Z. (2007), "Analysis of track irregularity spectrum of Shanghai-Nanjing railway", *J. Tongji Univ.*, **35**, 1342-1346. [In Chinese]
- Ma, L.H., Ni, P., Liang, Q.H. and Jiang, H. (2014), "Analysis on vertical profile irregularity of Shanghai-Nanjing intercity high-speed railway", *J. Beijing Jiaotong Univ.*, **38**(3), 50-54.
- Olmos, J.M. and Astiz, M.A. (2013), "Analysis of the lateral dynamic response of high pier viaducts under high-speed train travel", *Eng. Struct.*, **56**(6), 1384-1401.
- Poveda, E., Yu, R.C., Lancha, J.C. and Ruiz, G. (2015), "A numerical study on the fatigue life design of concrete slabs for railway tracks", *Eng. Struct.*, **100**, 455-467.
- Rocha, J.M., Henriques, A.A. and Calcada, R. (2014), "Probabilistic safety assessment of a short span high-speed railway bridge", *Eng. Struct.*, **71**, 99-111.
- Ruge, P., Widarda, D.R., Schmazlin, G. and Bagayoko, L. (2009), "Longitudinal track-bridge interaction due to sudden change of coupling interface", *Comput. Struct.*, **87**, 47-58.
- Shao, J.W., Zhao, D.X., Shu, L. and Shirley, J.D. (2016), "Safety and stability of light-rail train running on multispan bridges with deformation", *J. Bridge Eng.*, **21**(9), 06016004.
- Strauss, A., Wanwendner, R., Vidovic, A., Zambon, I. and Qiang, Y. (2017), "Gamma prediction models for long-term creep deformations of prestressed concrete bridges", *J. Civ. Eng. Manag.*, **23**(6), 681-698.
- Toydemir, B., Koçak, A., Sevim, B. and Zengin, B. (2017), "Ambient vibration testing and seismic performance of precast i beam bridges on a high-speed railway line", *Steel Compos. Struct., Int. J.*, **23**(5), 557-570.
- Tutumluer, E., Qian, Y., Hashash, Y., Ghaboussi, J. and Davis, D.D. (2013), "Discrete element modelling of ballasted track deformation behavior", *Int. J. Rail Transport.*, **1**, 57-73.
- Wang, K.P., Xia, H., Guo, W.W., Cao, Y.M. and Xuan, W.U. (2014), "Influence of uneven settlement of bridge piers on running safety of high-speed trains", *J. Vib. Shock*, **33**(6), 137-142.
- Yan, L. (2015), "Research on the Lateral Stability of the CRTS I Slab Track", M.S. Dissertation; Southwest Jiaotong University, Chengdu, China.
- Yan, B., Dai, G.L. and Hu, N. (2015), "Recent development of design and construction of short span high-speed railway bridges in China", *Eng. Struct.*, **100**, 707-717.
- Yang, S.C. and Jang, S.Y. (2016), "Track-bridge interaction analysis using interface elements adaptive to various loading cases", *J. Bridge Eng.*, **21**(9), 04016056.
- Yang, H., Chen, Z., Zhang, H. and Fan, J. (2014a), "Dynamic analysis of train-rail-bridge interaction considering concrete creep of a multi-span simply supported bridge", *Adv. Struct. Eng.*, **17**(5), 709-720.
- Yang, S., Xiao, H. and Huang, L.W. (2014b), "Effects on mechanical properties of track structure and running safety caused by uneven settlement of bridge pier", *Sensors Trans.*, **183**(12), 265-272.
- Zhang, J., Wu, D.J. and Li, Q. (2015), "Loading-history-based track-bridge interaction analysis with experimental fastener resistance", *Eng. Struct.*, **83**, 62-73.
- Zou, Z.H., Center, E.M. and Corporation, C.R. (2014), "Effects Analysis of Differential Settlement on Long-span Continuous Bridge and Ballastless Track Structure", *J. Railway Eng. Soc.*, (3), 61-65.

Nomenclature

The following symbols are used in this paper:

X_b	Longitudinal axis of bridge global coordinate system
Y_b	Vertical axis of bridge global coordinate system
Z_b	Lateral axis of bridge global coordinate system
X_s	Longitudinal axis of slab global coordinate system
Y_s	Vertical axis of slab global coordinate system
Z_s	Lateral axis of slab global coordinate system
X_r	Longitudinal axis of rail global coordinate system
Y_r	Vertical axis of rail global coordinate system
Z_r	Lateral axis of rail global coordinate system
x_{mb}	Longitudinal axis of the m -th girder local coordinate system
y_{mb}	Vertical axis of the m -th girder local coordinate system
z_{mb}	Lateral axis of the m -th girder local coordinate system
x_{ms}	Longitudinal axis of the m -th slab local coordinate system
y_{ms}	Vertical axis of the m -th slab local coordinate system
z_{ms}	Lateral axis of the m -th slab local coordinate system
a_m	Slope of the deformation function of the m -th slab
b_m	Constant
sum	Number of total fasteners
n	Number of fasteners on the m -th slab
P_{mi}	Force of the i -th fastener on the m -th slab
$R(x)$	Supporting force of CA mortar
F_{ml}	Force of the convex block on the left end of the m -th slab, $F_{ml} = k_t(z_{ms0} - z_{mb0})$
F_{mr}	Force of the convex block on the right end of the m -th slab, $F_{mr} = k_t(z_{ms(n+1)} - z_{mb(n+1)})$
P_{mk}	Fastener force at the k th fastener location of the m -th slab
k_t	Lateral tension and compression stiffness of convex block filler
k_{cz}	Lateral stiffness of mortar layer
P_k	Fastener forces on rails
$[Z_{ms}]$	Matrix of lateral deformations of the m -th slab at all fastener locations
$[A_m]$	Influence matrix of fastener lateral forces of the m -th slab
$[T_m]$	Influence matrix of bridge lateral deformations for the m -th slab deformations

$[\mathbf{P}_m]$	Matrix of fastener lateral forces of the m -th slab
$[\mathbf{Z}_s]$	Matrix of lateral deformations of $M \times N$ slabs at all fastener locations
$[\mathbf{A}]$	Influence matrix of fastener forces for slab lateral deformations
$[\mathbf{P}]$	Matrix of fastener lateral forces
$[\mathbf{T}]$	Influence matrix of bridge lateral deformations
$[\mathbf{Z}_r]$	Matrix of rail lateral deformations at all fastener locations
$[\mathbf{H}]$	Influence matrix of fastener forces on rail lateral deformations
$[\mathbf{I}]$	Unit matrix of sum -order
k_{fz}	Lateral stiffness of fastener
φ_{r0}	Rotating angle of rail at $X_r = 0$ section
Q_{r0}	Shear force of rail at $X_r = 0$ section
EI_{rz}	Lateral flexural rigidity of rail
Z_{rt}	Lateral deformation of rail at $X_r = l_i$ section